Imaging the Infrared Multiphoton Excitation and Dissociation of Propargyl Chloride

Journal:	*Physical Chemistry Chemical Physics*
Manuscript ID	CP-ART-10-2018-006668.R1
Article Type:	Paper
Date Submitted by the Author:	04-Dec-2018

Complete List of Authors:	Foley, Casey; University of Missouri Columbia College of Arts and Science, Chemistry Alavi, S. Tahereh; University of Missouri Columbia College of Arts and Science, Chemistry Joalland, Baptiste; University of Missouri Columbia College of Arts and Science, Chemistry Broderick, Bernadette; University of Missouri Columbia College of Arts and Science, Chemistry Dias, Nureshan; University of Missouri Columbia College of Arts and Science, Chemistry Suits, Arthur; University of Missouri Columbia College of Arts and Science, Chemistry

SCHOLARONE™
Manuscripts

Imaging the Infrared Multiphoton Excitation and Dissociation of Propargyl Chloride

Casey D. Foley, S. Tahereh Alavi, Baptiste Joalland, Bernadette M. Broderick, Nureshan Dias and Arthur G. Suits*

Department of Chemistry
University of Missouri, Columbia MO 65211

Abstract

Infrared multiphoton excitation is combined with UV excitation and state-resolved probes of $Cl(^2P_{3/2})$, $Cl^*(^2P_{1/2})$, and HCl to study the photochemistry of propargyl chloride. The results show evidence both of infrared multiphoton dissociation on the ground electronic state and infrared multiphoton excitation followed by UV dissociation. The results are interpreted with the aid of a full characterization of the stationary points on the ground state using ab initio methods, as well as our recent experimental and theoretical characterization of the UV photochemistry of the molecule. The data suggest elimination of HCl on the ground electronic state produces linear propadienylidene as a coproduct over a roaming-like transition state that accesses the Cl-H-C abstraction geometry. This identification is supported by separate chirped-pulse microwave studies in a quasi-uniform flow also reported here.

*suitsa@missouri.edu

Introduction

High-power line-tunable TEA-CO_2 lasers stimulated the emergence of infrared multiphoton dissociation (IRMPD) studies in the 1970s and 1980s.[1-10] This permitted the investigation of ground state unimolecular decomposition of molecules under collisionless conditions in molecular beams.[11-16] Although applied with considerable success to reveal the global features of these processes, the methods were in wide use prior to the development of state-selected velocity map imaging techniques.[17-19] The latter method is capable of extremely high velocity resolution and at the same time quantum state-specific product detection, affording deep insight into photochemical processes in favorable cases.[20-24]

Our interest in combining IRMPD with imaging is inspired in part by a desire to explore roaming radical reactions in detail. These are reactions, exemplified by formaldehyde most notably, that involve frustrated dissociation toward radicals in which the system instead returns to give closed-shell products, usually after an excursion to a long-range, high potential energy region of the surface.[19, 25, 26] First characterized in detail in formaldehyde and acetaldehyde,[13] it is now generally seen as a universal aspect of chemical reactivity, with very active theoretical efforts to interpret it in terms of transition state theory,[27-29] including recent phase space treatments,[30, 31] and an alternative approach adapted from the condensed phase.[32] Although NO_3 dissociation clearly showed the importance of roaming in the excited electronic state,[16, 33] in general roaming reactions are more easily seen and characterized on the ground electronic state. IRMPD combined with velocity map imaging thus offers a means to explore this novel aspect of reaction dynamics in detail.

Recently, we began adapting IRMPD for high resolution DC slice imaging applications.[16, 34-36] In IRMPD of vinyl chloride, for example, state-resolved HCl detection showed both modest rotational excitation and very low translational energy release, consistent with 3-center HCl elimination producing cold vinylidene as a coproduct.[35] Propargyl chloride experiments have primarily sought to determine the branching of dissociation channels that originate from the strong excitation near 193 nm.[37-39] Butler and coworkers summarized photodissociation of propargyl chloride and other halogenated hydrocarbons in their imaging study in 2006.[37] C-Cl bond fission products were found to branch to Cl and Cl* equally and slow translational energy peaks were determined to not be the result of HCl fragmentation as previously thought. We recently presented an imaging investigation at longer UV wavelengths that used multireference calculations to characterize the electronic excitations of propargyl chloride from 5.0 to 8.0 eV.[40] A high density of singlet and triplet excited electronic states were identified and complex, repulsive dissociation dynamics were observed with both direct and predissociation processes. At 236 nm three distinct triplet excited states were accessed giving distinct features in the images. A slow component producing exclusively ground state products with a parallel angular distribution was assigned to T_1. Evidence for T_2 and T_3 excitations were also seen in a fast peak comprising distinct perpendicular and parallel components, respectively. Furthermore, T_2 and T_3 preferentially branched to spin-orbit excited and ground state Cl, respectively. Evidence was also seen for predissociation of a bound S_1 state accessed when propargyl chloride was excited at 212 nm. Here, we combine infrared multiphoton excitation (IRMPE) of propargyl chloride with state-

specific detection using REMPI with DC slice imaging to examine the dynamics of dissociation both on the ground state near threshold and in vibrationally mediated photodissociation through these electronically excited states. The experimental data is interpreted using theoretical calculations to determine minima and transition states *en route* to products and aid in identifying the C_3H_2 product isomer formed. We also performed complementary chirped-pulse mm-wave spectroscopy experiments in a quasi-uniform flow (CPUF) which support the computational identification of the C_3H_2 product isomer as the linear propadienylidene species.

Experimental and Theoretical Methods

DC Slice Imaging

The experimental method and apparatus were previously reported,[41] but a brief description of relevant information is included here. The apparatus consists of source and detection chambers separated by an aluminum plate on which a skimmer is mounted. Each chamber is pumped by a separate turbomolecular pump. A molecular beam of propargyl chloride, C_3H_3Cl, was introduced into the source chamber via a pulsed solenoid valve (Parker-General) and subsequently skimmed and supersonically expanded. 7% C_3H_3Cl was generated by passing helium through C_3H_3Cl in a bubbler at 0°C. IR radiation from a grating-tuned TEA-CO_2 at 10.44 μm was used to excite C_3H_3Cl by strong absorption via the C-C stretch. A 35 cm focal length ZnSe lens was used to focus the measured ~650 mJ per pulse (fluence 7.2 J/cm^2) onto the molecular beam slightly upstream of the UV laser. The IR beam was fired ~800 ns before the UV beam.

UV radiation around 241 nm and 0.8 mJ/pulse was focused onto the molecular beam slightly downstream from the IR laser beam with a UV fused silica lens and used to ionize HCl by (2+1) REMPI via the R and S branches of the $F^1\Delta_2 \leftarrow\leftarrow X\ ^1\Sigma^+$.[42] Unlike other transitions in this region, this REMPI transition exclusively produces HCl^+. For the Cl detection experiments, UV radiation near 235 nm was focused onto the molecular beam with a 30 cm focal length fused silica lens. These wavelengths were chosen for specific Cl($^2P_{3/2}$) and Cl*($^2P_{1/2}$) REMPI transitions. For Cl detection the transition was $2D^0_{3/2} \leftarrow 2P^0_{3/2}$ (84988.48 cm^{-1}), while for Cl* the transition was $2P^0_{3/2} \leftarrow 2P^0_{1/2}$ (85442.43 cm^{-1}). In each case, the wavelength was scanned repeatedly across the Doppler profile while recording the images. All UV light was polarized vertically, parallel to the plane of the detector. The resulting ions were accelerated by an ion optics assembly through a time-of-flight tube toward a pulsed 75 mm microchannel plate detector (BOS-75-OPT01, Beam Imaging Solutions) coupled to a P-47 phosphor screen for DC slice ion imaging. Images were captured using a USB CCD camera and in-house data acquisition software NuACQ. Time-of-flight information was obtained with a photomultiplier tube monitoring the phosphor screen. The experiment was performed at 10 Hz. Image reconstruction and data extraction were done using our finite slice analysis method, FinA.[43, 44]

Chirped-Pulse Quasi-Uniform Flow Spectroscopy

The experimental method and apparatus were previously reported, but a brief description of relevant information is included here.[45-48] The chirped-pulse mm-wave spectrometer covering the range 70-90 GHz is coupled to a pulsed quasi-uniform flow as described previously. The propargyl chloride is seeded at 1% in helium and expanded from a Laval nozzle forming a quasi-

uniform flow at a total density of ~10^{16} cm^{-3} and a temperature of 10 to 40 K. Photodissociation of the propargyl chloride by a loosely focused 193nm laser beam (<10 mJ/pulse) gives several products including the propargyl radical with Cl atoms, and HCl with C_3H_2. Absorption of a second 193 nm photon by the propargyl radical also gives C_3H_2 products, and the isomer-specific branching is the subject of studies reported elsewhere. The photoproducts are internally cooled in the flow, after which they are excited by $\pi/2$ pulses of mm-wave radiation tuned to known transitions of C_3H_2 isomers at intervals of 10 μs. After each mm-wave pulse, the free induction decay of the excited molecules is acquired and accumulated in the time domain, then Fourier-transformed to give the rotational spectrum from which branching is determined as described previously. Results for propargyl chloride shown here are compared to results obtained previously for 1,2-butadiene to isolate the component that is associated with HCl elimination.

Theoretical Calculations

To explore the ground state potential energy surface of the C_3H_3Cl system, we employed the DFT functional wB97XD,[49] which incorporates an empirical correction for long-range interactions, in conjunction with the aug-cc-pVDZ basis set.[50-52] Further calculations were performed using the composite CBS-QB3 method.[53-55] The structures of the minima and transition states were fully optimized and their vibrational frequencies estimated within the harmonic approximation[53, 56] The transition states found in each pathway were confirmed by intrinsic reaction coordinate calculations. All calculations were performed with the Gaussian 16W package.[56] Associated files are provided in the supplementary information.

Results and Discussion

DC Slice Imaging

Ground state Cl atom images from photodissociation of propargyl chloride near 235 nm are first presented. Figure 1A shows a DC slice image obtained with the UV probe laser alone ("1-color") and Fig. 1B shows probe following the high-power CO_2 laser pulse ("2-color"). The 1-color image is bimodal with a broad inner ring and a sharper outer ring with recoil along the laser polarization direction. We recently determined that the inner and outer rings were the result of excitation to triplet states of propargyl chloride, namely T_1 and T_2/T_3, respectively. We discuss the mixed composition of the outer ring further below.

The 2-color image shows profound changes. The total signal increases by roughly a factor of two and a varying enhancement is seen in the yield at all recoil energies, with the central region becoming very intense. It is clear this enhancement must be due, in large part, to IR-enhanced UV dissociation, since the enhancement closely follows the distributions we observed in the UV-only images. The effects may be seen more clearly in the translational energy distributions displayed in Figure 2A. The region we assigned previously to the T_1 excitation near 10 kcal/mol is enhanced by ~30%, while the main T_2/T_3 peak is not strongly enhanced. Instead, the distribution extends to a significantly higher limiting translational energy: rather than the sharp cutoff around 35 kcal/mol, the distribution tails off slowly to greater than 50 kcal/mol. Considering this entire

distribution there is a similar large IR enhancement for the T_2/T_3 contribution but it is spread over a broad, higher energy range.

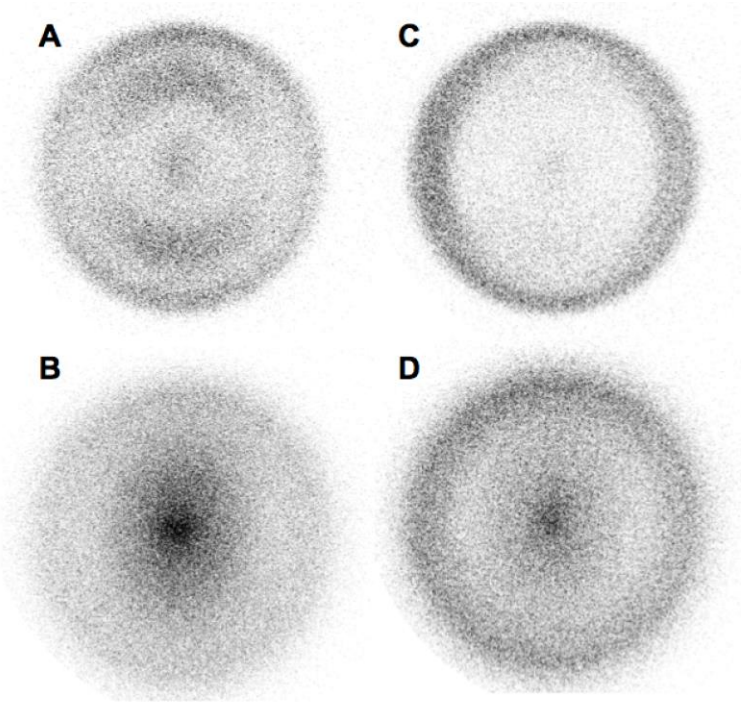

Fig. 1: DC slice images of 1-color UV Cl (A), 2-color Cl (B), 1-color UV Cl* (C), and 2-color Cl* from photodissociation of propargyl chloride. Laser polarization axis is vertical in the plane of the figure.

We previously examined energy partitioning in the UV-only dissociation and found for the main peak that ~45% of the available energy appeared in translation. If this fraction is maintained for this IR enhanced dissociation, then we can infer that the maximum excitation of the molecules that undergo IR enhanced dissociation via the T_2/T_3 excitation is ~42 kcal/mol, i.e., on the order of 16 IR photons. Interestingly, we do not see such a shift in the maximum translational energy for the T_1 contribution. This is likely due to the fact that the C-Cl coordinate on T_1 surface is not as steeply sloped in the Franck-Condon region compared to T_2/T_3, so additional vibrational energy does not yield a greater impulse. Additional vibrational excitation does, however, increase the Franck-Condon envelope to give greater excitation probability. The other very notable feature of the 2-color vs. 1-color images and translational energy distributions for Cl is the prominent low energy peak that only appears in the 2-color result. This is a peak near 5 kcal/mol that we ascribe to IRMPD leading to Cl atom elimination with the UV serving only as probe.

Analogous results for Cl* are shown in the Figure 1C and D images, showing marked differences from the ground state Cl case. The 1-color Cl* image does not show the 10 kcal/mol contribution assigned to T_1 excitation. It also shows an interesting structure in the main peak that is perpendicular for the inner component and parallel for the outer component, as discussed previously. We assigned the inner component to the T_2 excitation and the outer component to T_3 and argued that the former branches more to Cl*, accounting for the more strongly perpendicular aspect of the inner component of the main peak for Cl* compared to Cl. The 2-color results for Cl* also show new and enhanced dissociation processes. There is a slight enhancement of the peaks corresponding to T_2 and T_3, and again a strong broad feature extending to 50 kcal/mol or so. The Cl* data also exhibits a low energy feature around 5 kcal/mol consistent with IRMPD.

The Cl and Cl* images indicate dissociation by IRMPD and concurrent IR-enhanced UV photodissociation. Analysis of the angular distributions at different regions of the image further assists in disentangling the contribution from each. These are fitted to the expression:[57, 58]

$$I(\theta) \propto 1 + \beta(P_2(\cos\theta))$$

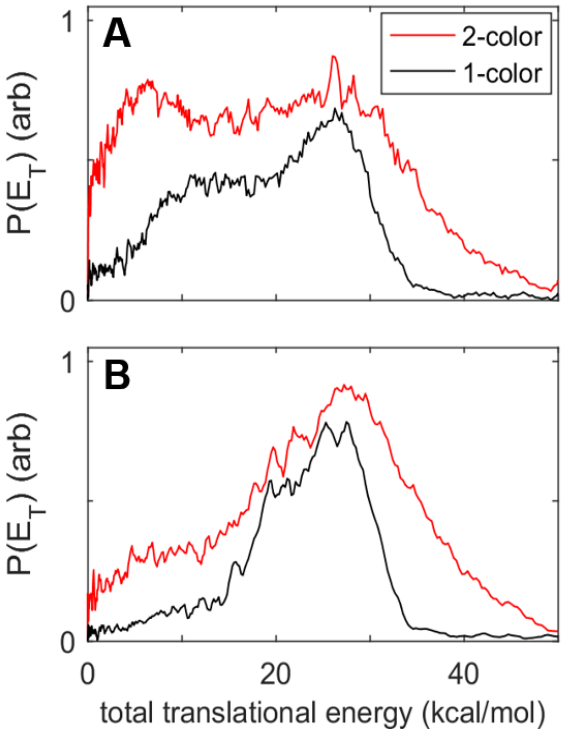

Fig. 2: Translational energy distributions of Cl (A) and Cl* (B) from 1-color UV (black) and 2-color (red) photodissociation of propargyl chloride photodissociation.

dissociation from the rotating parent molecule and from a wider range of geometries. For the region of the main peak around 20 kcal/mol that we associate primarily with T_2 excitation, there is little impact on the anisotropy although there is a significant enhancement in the signal. One possible explanation is that the excitation shifts more to T_3 which is more parallel, but at the same time there is a reduction in overall anisotropy, and these effects cancel. In the region of the main peak associated with T_3, we again see a significant reduction in anisotropy, from β ~0.7 to 0.3. However, beyond 35 kcal/mol, the β value rises significantly, to

with P_2 the second Legendre polynomial. β is given as a function of recoil energy in Figs. 3 and 4. We reproduce the translational energy distributions in these plots to facilitate the comparison. Fig. 3A gives the 1-color result for Cl, Fig. 3B gives the 2-color result. The low translational energy release and nearly isotropic angular distribution of the image center supports the assignment of the slow component to IRMPD. The IR-enhanced photodissociation distribution which we assign to T_1 shows a reduction in the anisotropy from β ~0.7 to ~0.4. We attribute this to rovibrational excitation of the parent induced by the CO_2 laser leading to

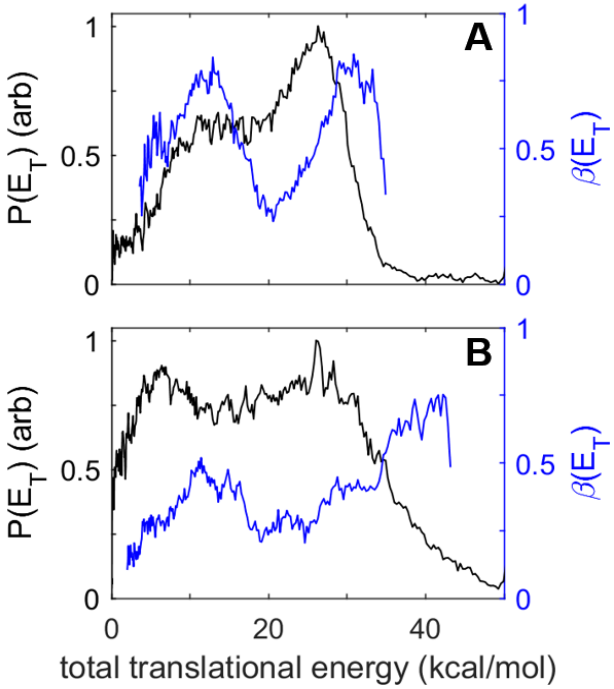

Fig. 3: Translational energy distributions (black) and anisotropy parameter β (blue) of Cl from 1-color UV (A) and 2-color (B) photodissociation of propargyl chloride.

about 0.8. We believe this indicates a contribution from S_2 now making an appearance, as direct excitation from distorted geometries becomes possible. S_2 is the first strongly allowed transition. The Cl* angular distributions given in Fig. 4A and 4B also show a significant reduction in overall anisotropy. The peak associated with T_2 changes from β ~-0.4 to 0.1. The main peak associated with T_3 shows only a modest reduction in anisotropy, while again the new signal beyond 32 kcal/mol shows an increase in β just as in the case of Cl, again suggesting access to S_2 for these hot molecules.

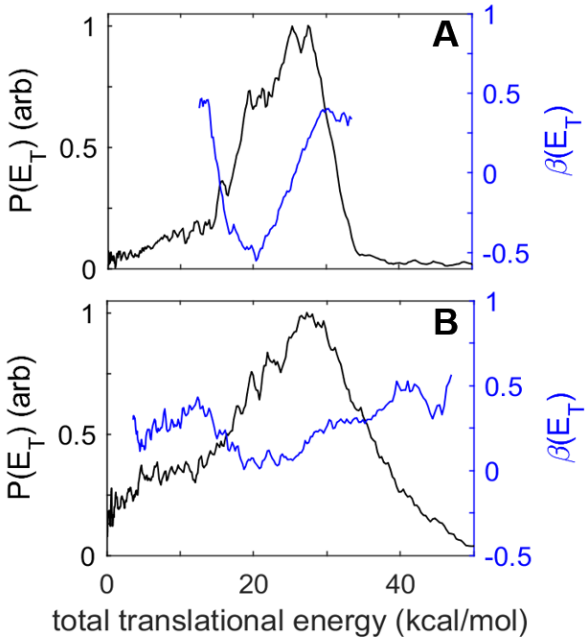

Fig. 4: Translational energy distributions (black) and anisotropy parameter β (blue) of Cl* rom 1-color UV (A) and 2-color (B) experimental configurations of propargyl chloride photodissociation.

Initial excitation by intense IR light gives access to unexplored parts of the potential energy surfaces, both in IRMPD and IR-enhanced UV photodissociation. The key difference between the two is that for IRMPD, we exclusively study dissociation from the ground electronic state. Previously, we reported that UV photodissociation at 235 nm does not yield HCl elimination and ascribed this to processes involving largely repulsive excited states. With IRMPD, however, we find evidence that the HCl elimination channel opens up, as we detect HCl state-selectively for the first time.

The HCl rotational distribution was obtained by scanning the probe laser after the IR excitation. The experimental REMPI spectrum can be seen in the top trace of Fig. 5 with HCl products detected on the S and R branches of the F $^1\Delta_2$ $X^1\Sigma^+$ (0,0) transition. Unfortunately, the spectrum is quite noisy owing to non-resonant background signals in which there is also some regular oscillation from etalon effects at a window. By modeling the relative abundance of the rotational population using PGOPHER (bottom trace Fig.5),[59, 60] we inferred that HCl fragments were produced very cold with a rotational temperature of ~85 K.

We have also recorded HCl images on several transitions and we show the results for R(1) in Fig. 6A. The image shows an intense central spot tapering to very low intensity that extends at considerable distance from the image center. Analysis of the image after subtraction of the background signal gives the distributions in Fig. 6B. The $P(E_T)$ shows a peak at very low translational energy, near 1 kcal/mol, dropping quickly to around 10 kcal/mol, after which there is a tail out to ~60 kcal/mol. This clearly appears to consist of two components: one of these peaks at low energy typical of a ground state, barrierless dissociation, while the other encompasses a broad distribution such as over a barrier or from an excited state process. We have fitted it to a sum of two distributions each using a flexible form that readily represents these two components:

$P(E_T) = a(E_T/E_{Tmax})^b(1- E_T/E_{Tmax})^c$

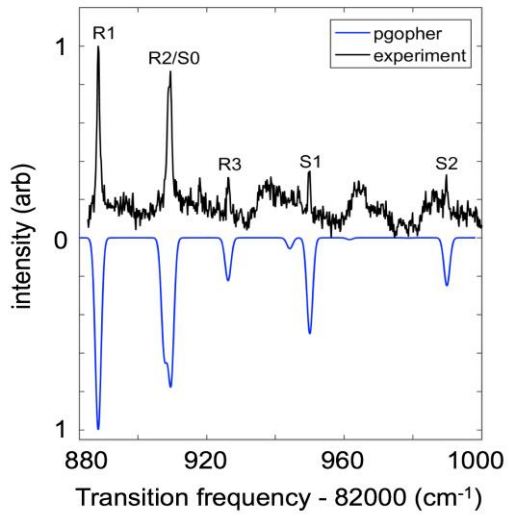

Fig. 5: Experimental HCl IRMPD REMPI spectrum (top trace) and simulation at 85 K (bottom trace).

bimodal with a minor peak at low translational energy and a broad one extending to 60 kcal/mol or so, much as we see here. However, their low energy peak was roughly ten-fold lower than what is seen here. We have argued above that initial vibrational excitation gains direct access to S_2, so it is reasonable to expect a component in our HCl distribution that also resembles the 193 nm result which was assigned to S_2. We suggest that the slow component is ground state dissociation, mostly from direct IRMPD, but there may be a small contribution from internal conversion from S_2 that would also account for the analogous peak in the 193nm result. The broad fast component is then entirely due to IR-enhanced UV dissociation through S_2. This is confirmed by the angular distributions which are close to isotropic at low recoil energy but become predominantly parallel in the region of the dissociation attributed to S_2. One question that arises is how we could obtain a and the result is shown in red in Fig. 6B. Also shown in Fig. 6B is the recoil-dependent angular distribution summarized as $\beta(E_T)$. It is very illuminating to examine this in light of results from Butler and coworkers at 193nm. They exerted considerable effort to distinguish the contributions of C_3^+ (m/z=36) from C_3H_3 fragmentation in the electron impact ionizer to the HCl^+ signal at the same mass-to-charge ratio. They concluded that the HCl elimination P(E) is

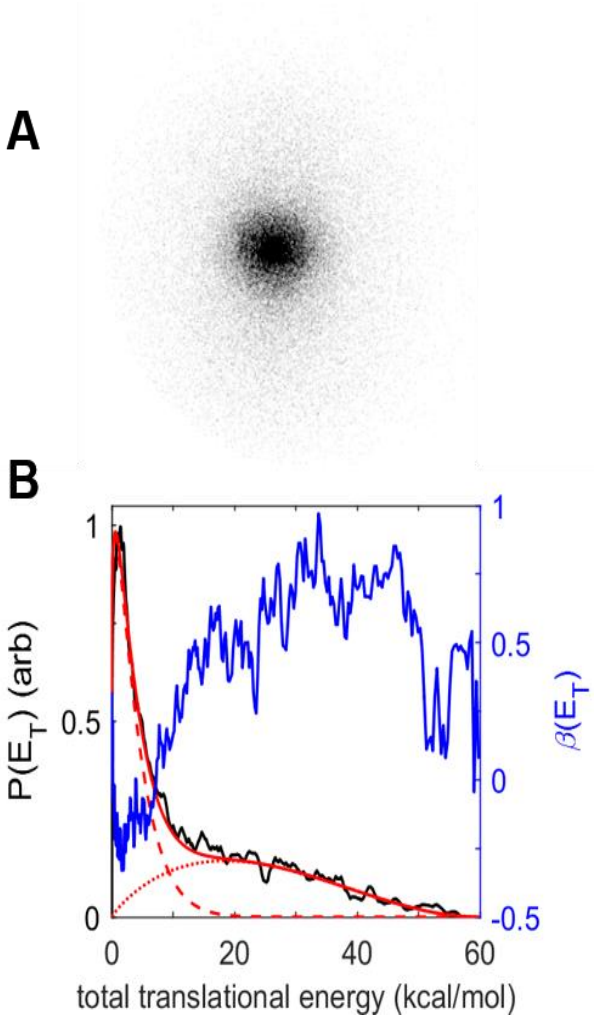

Fig. 6: DC slice image of HCl (v=0,j=1) (A) and translational energy distribution (black) and anisotropy parameter β (blue) (B) from 2-color photodissociation of propargyl chloride. Red lines show decomposition of the distribution to two components (see text.)

rotational temperature of 85 K given the broad component of the translational energy distribution that extends to such high energy. To fit both we would clearly require two different rotational temperatures. Unfortunately, the high translational energy distribution associated to the S_2 contribution is likely so Doppler broadened that it is lost in the considerable noise in the REMPI spectrum, and we only detect the intense features near line centers that are associated to the IRMPD.

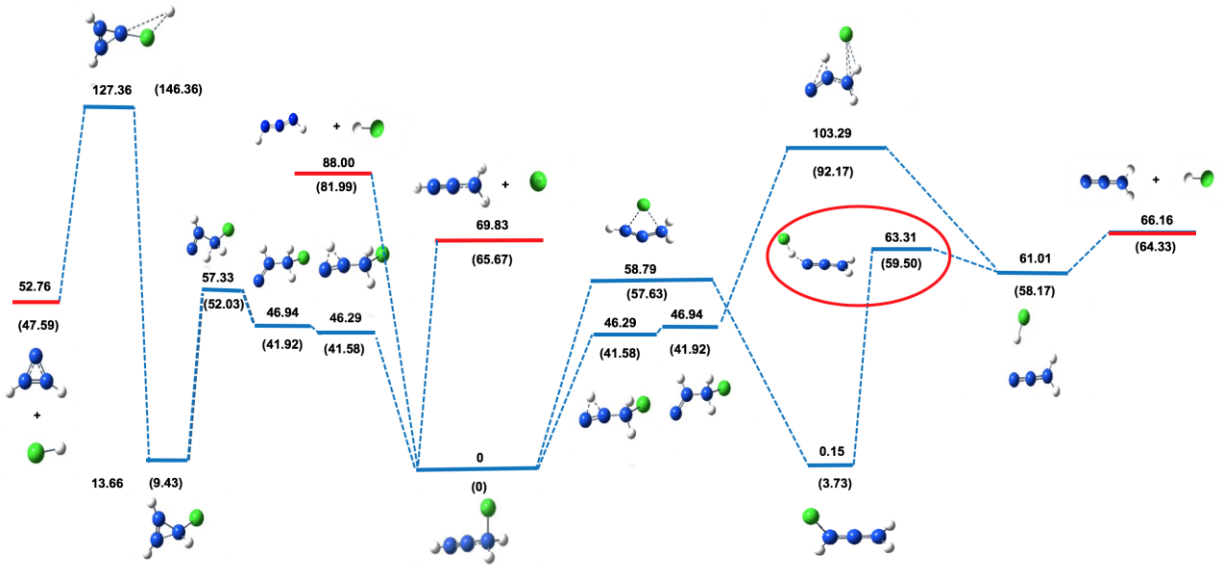

Fig. 7: Relative energies (in kcal/mol) of stationary points on the ground state singlet potential energy surface of C_3H_3Cl, including zero-point energy correction. The roaming TS is encircled in red. Values are from CBS-QB3 calculations and, in parentheses, from wB97XD/aug-cc-pVDZ calculations.

In our previous study we examined the excited state potential surfaces in some detail. Here, to aid in understanding the IRMPD, we characterize stationary points on the ground electronic state. The relative zero-point energies of all structures are shown in Figure 7. The threshold for Cl elimination is calculated to be 69.8 kcal/mol, in reasonable agreement with the value from the Active Thermochemical Tables of 68.6.[61, 62] Four different pathways have been identified for HCl elimination to aid in understanding the dynamics of that process. Two of these lead to formation of linear propadienylidene (l-C_3H_2) and another pathway gives cyclic propadienylidene (c-C_3H_2) as the co-product of HCl, while a fourth gives singlet propargylene. The barrier for elimination giving the cyclic product is prohibitively high at 127 kcal/mol. There is a pathway for direct HCl elimination from propargyl chloride giving l-C_3H_2 with a barrier of 103 kcal/mol. Direct HCl loss to form singlet propargylene, HCCCH, is also possible as shown. We were unable to locate a transition state for this and conclude it is barrierless and endoergic by 88 kcal/mol. Alternatively, isomerization to 1-chloroallene has a barrier of only 58.8 kcal/mol, after which there is dissociation at 66 kcal/mol. This is the lowest energy decomposition pathway. In this pathway two transition states are found: one corresponding to the isomerization to 1-chloroallene and the other to HCl formation from 1-chloroallene leading to a van der Waals well. The second

transition state separating 1-chloroallene and the well, highlighted in Fig. 7, has the Cl atom in an abstraction geometry rather than a 3-center or 4-center HCl elimination structure. This is much as what we have seen for HCl elimination in Cl + butene reactions, for which only TSs of roaming character connect the strongly bound adducts to the elimination of HCl at the allylic sites.[63, 64] That is, the Cl atom has to come off of 1-chloroallene to attain the abstraction geometry. This view is supported by the energy of the TS that is near that of the dissociated radical pair, as well as its low vibrational frequencies: The TS has an imaginary frequency of -193.35 cm^{-1} and two low bound frequencies of 72.76 and 196.20 cm^{-1}.

Chirped-Pulse Quasi-Uniform Flow Detection of C_3H_2

To support our identification of the C_3H_2 structure, we examined the 193nm photodissociation of propargyl chloride in our CPUF apparatus, and the results are shown in Fig. 8. Although this is a different wavelength from that employed in the imaging study above, in both cases we believe the HCl results from dissociation on the ground state so we expect the same product isomer.

Results for propargyl chloride are presented along with those for 1,2 butadiene that we previously studied to understand branching in propargyl radical dissociation. These experiments were performed in a quasi-uniform flow at low temperature but in a collisional environment to permit relaxation of the products to the local temperature (~ 14 K) for detection. In our previous study, propargyl radical was first prepared by photodissociation of 1,2-butadiene. Absorption of a second photon gives the radical products which are then cooled in the flow and detected. In Fig. 8a we show representative raw signals on the indicated rotational transitions for l-C_3H_2 and c-C_3H_2 but additional transitions are included and averaged (after normalizing by the density and weighting by the linestrength) to give the branching, l-C_3H_2 /(l-C_3H_2 + c-C_3H_2), shown in Fig. 8b. The red spectra indicate times in the flow we associate with nascent photochemical products after cooling to the flow temperature, 60-70 μs after the photolysis laser. We attribute the intensity and time-dependence of C_3H_2 signals from 1,2-butadiene exclusively to H atom loss from propargyl radical, with negligible contribution of CH_4 loss from the parent molecule. Also shown in Fig. 8 is the analogous result for propargyl chloride photodissociation. Although

propargyl chloride does produce propargyl radical that can subsequently undergo the same chemistry, C_3H_2 products are also clearly formed directly by HCl loss from the propargyl chloride parent as discussed extensively in the literature. Thus, the two precursors give rise to different branching fractions between the C_3H_2 isomers. In addition to H atom loss from the propargyl radical that occurs for both propargyl chloride and 1,2 butadiene, for the former there is also direct HCl elimination. The increased branching to linear over cyclic-C_3H_2 seen in Fig. 8 shows that l-C_3H_2 is the dominant isomer formed following HCl elimination from propargyl chloride. Subsequent disappearance of l-C_3H_2 and appearance of intense c-C_3H_2 (after 70 μs) is ascribed to H-atom catalyzed isomerization in the high-density region of the flow as discussed previously.[65]

Singlet propargylene is also a possible product isomer, but we cannot detect it owing to its negligible dipole moment. We would expect this to undergo H catalyzed isomerization to c-C_3H_2, which would appear at later times, just as we have shown for the triplet propargylene and l-C_3H_2. We actually observe much less of the late c-C_3H_2 from H-catalyzed isomerization in the case of propargyl chloride. This may reflect secondary chemistry involving Cl atoms, but in any case it does not suggest the presence of a distinct dark channel. The much higher energy onset of HCCCH

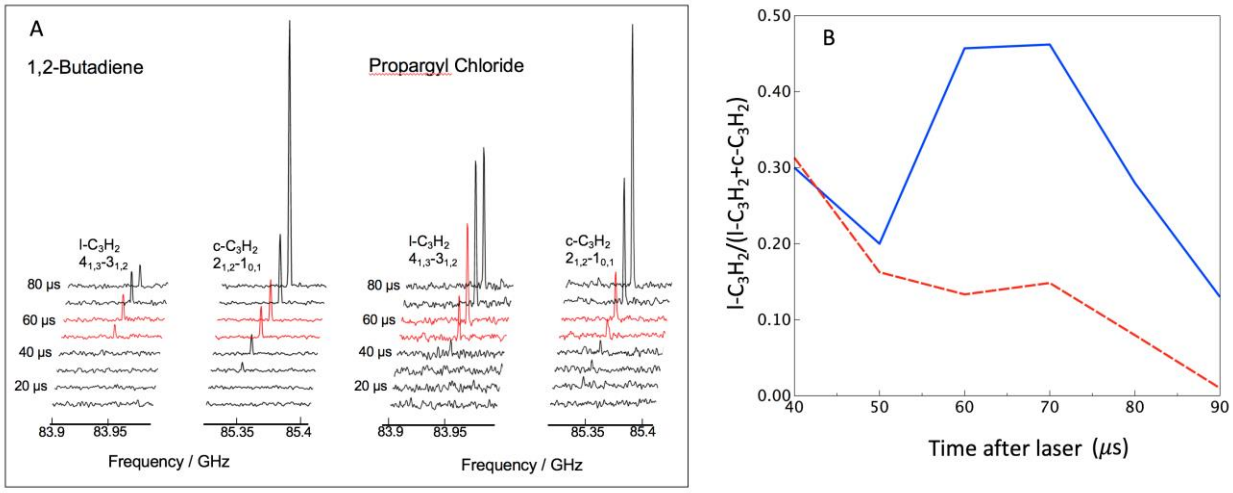

Fig. 8: CPUF rotational spectra for indicated C_3H_2 isomers following 193nm photodissociation of 1,2-butadiene and propargyl chloride (A). Branching to l-C_3H_2 for propargyl chloride (blue solid line) or 1,2-butadiene (red dashed line) (B).

also suggests it would be weak or negligible relative to the HCl loss from chloroallene under conditions of IRMPD. Although we can readily determine the branching between the different isomers detected, we do not know the probability of direct propargyl chloride photodissociation vs. absorption of a second photon by the propargyl radical, so we cannot determine the branching for HCl elimination from this data. In short, these rotational spectra for propargyl chloride photodissociation at 193nm show enhanced formation of l-C_3H_2 compared to 1,2 butadiene, supporting it assignment as the product isomer as identified in the ab initio calculations.

Conclusions

Translational energy distributions of Cl fragments reveal dissociation from multiple pathways, including UV, IR-enhanced UV, and IRMPD processes in these expeirments. IRMPE results in the enhancement of UV photodissociation processes and additional fast fragments and parallel anisotropy which we attribute to access to S_2 from distorted geometries. IRMPD produces a high abundance of slow Cl fragments and less slow Cl* fragments. We interpret these fragments peaking at low energy to be the result of dissociation near threshold from the ground state. HCl is likely formed both by IRMPD, peaking at low energy, and from S_2 extending to 60 kcal/mol. A quantum chemical survey of the ground state PES indicates that the lowest energy decomposition pathway involves isomerization to 1-chloroallene followed by a roaming-like transition state that assumes an abstraction geometry to produce HCl and l-C_3H_2. This is in line with the cold rotational temperature measured for the low energy peak. CPUF experiments, although performed at 193 nm, further support the production of l-C_3H_2 in photodissociation of propargyl chloride. Results presented here combined with our recent characterization of its UV photodissociation provide an improved understanding of the potential energy landscape and associated dissociation dynamics of propargyl chloride.

SUPPORTING INFORMATION DESCRIPTION

Geometries and intrinsic reaction coordinate calculations are provided.

Acknowledgement

This work was supported by the Army Research Office under award number W911NF-17-1-0099.

References

1 A. J. Beaulieu, *Appl. Phys. Lett.*, 1970, **16**, 504-505.
2 O. R. Wood, R. L. Abrams and T. J. Bridges, *Appl. Phys. Lett.*, 1970, **17**, 376-378.
3 J. A. Beaulieu, *P. IEEE*, 1971, **59**, 667-674.
4 R. L. Abrams and O. R. Wood, *Appl. Phys. Lett.*, 1971, **19**, 518-520.
5 Y.-L. Pan, A. F. Bernhardt and J. R. Simpson, *Rev. Sci. Instrum.*, 1972, **43**, 662-666.
6 F. M. Lussier and J. I. Steinfeld, *Chem. Phys. Lett.*, 1977, **50**, 175-180.
7 P. A. Schulz, A. S. Sudbcent, D. J. Krajnovich, H. S. Kwok, Y. R. Shen and Y. T. Lee, *Ann. Rev. Phys. Chem.*, 1979, **30**, 379-409.
8 E. J. Hintsa, A. M. Wodtke and Y. T. Lee, *J. Phys. Chem.*, 1988, **92**, 5379-5387.
9 A. M. Wodtke, E. J. Hintsa and Y. T. Lee, *J. Phys. Chem.*, 1986, **90**, 3549-3558.
10 G. Hancock and K. G. McKendrick, *J. Phys. Chem.*, 1988, **92**, 1839-1846.
11 A. S. Sudbo/, P. A. Schulz, E. R. Grant, Y. R. Shen and Y.-T. Lee, *J. Chem. Phys.*, 1979, **70**, 912-929.
12 A. M. Wodtke, E. J. Hintsa and Y. T. Lee, *J. Chem. Phys.*, 1986, **84**, 1044-1045.
13 P. L. Houston and S. H. Kable, *P. Natl. Acad. Sci.*, 2006, **103**, 16079-16082.
14 N. Herath and A. G. Suits, *Ann. Rev. Phys. Chem.*, 2011, **2**, 642-647.
15 J. M. Bowman and B. C. Shepler, *Ann. Rev. Phys. Chem.*, 2011, **62**, 531-553.
16 R. Fernando, A. Dey, B. M. Broderick, B. Fu, Z. Homayoon, J. M. Bowman and A. G. Suits, *J. Phys. Chem. A*, 2014, **119**, 7163-7168.
17 D. W. Chandler and P. L. Houston, *J. Chem. Phys.*, 1987, **87**, 1445-1447.
18 A. e. Eppink, T. J. B. and D. H. Parker, *Rev. Sci. Instrum.*, 1997, **68**, 3477-3484.
19 D. Townsend, S. A. Lahankar, S. K. Lee, S. D. Chambreau, A. G. Suits, X. Zhang, J. Rheinecker, L. B. Harding and J. M. Bowman, *Science*, 2004, **306**, 1158-1161.
20 E. R. Grant, M. J. Coggiola, Y. T. Lee, P. A. Schulz, A. S. Sudbo and Y. R. Shen, *Chem. Phys. Lett.*, 1977, **52**, 595-599.
21 A. S. Sudbo/, P. A. Schulz, Y. R. Shen and Y. T. Lee, *J. Chem. Phys.*, 1978, **69**, 2312-2322.
22 F. Huisken, D. Krajnovich, Z. Zhang, Y. R. Shen and Y.-T. Lee, *J. Chem. Phys.*, 1983, **78**, 3806-3815.
23 X. Zhao, E. J. Hintsa and Y. T. Lee, *J. Chem. Phys.*, 1988, **88**, 801-810.
24 C. A. Longfellow and Y. T. Lee, *J. Phys. Chem.*, 1995, **99**, 15532-15537.
25 A. G. Suits, *Acc. Chem. Res*, 2008, **41**, 873-881.
26 M. S. Quinn, D. U. Andrews, K. Nauta, M. J. Jordan and S. H. Kable, *J. Chem. Phys.*, 2017, **147**, 013935.
27 L. B. Harding, S. J. Klippenstein and A. W. Jasper, *J. Phys. Chem. A*, 2012, **116**, 6967-6982.
28 L. B. Harding, S. J. Klippenstein and A. W. Jasper, *Phys. Chem. Chem. Phys.*, 2007, **9**, 4055-4070.
29 S. J. Klippenstein, Y. Georgievskii and L. B. Harding, *J. Phys. Chem. A*, 2011, **115**, 14370-14381.
30 F. A. Mauguière, P. Collins, Z. C. Kramer, B. K. Carpenter, G. S. Ezra, S. C. Farantos and S. Wiggins, *Ann. Rev. Phys. Chem.*, 2017, **68**, 499-524.

31 F. d. r. A. Mauguière, P. Collins, Z. C. Kramer, B. K. Carpenter, G. S. Ezra, S. C. Farantos and S. Wiggins, *J. Phys. Chem. Lett.*, 2015, **6**, 4123-4128.

32 D. V. Cofer-Shabica and R. M. Stratt, *J. Chem. Phys.*, 2017, **146**, 214303.

33 M. P. Grubb, M. L. Warter, A. G. Suits and S. W. North, *J. Phys. Chem. Lett.*, 2010, **1**, 2455-2458.

34 A. Dey, R. Fernando, C. Abeysekera, Z. Homayoon, J. M. Bowman and A. G. Suits, *J. Chem. Phys.*, 2014, **140**, 054305.

35 R. Fernando, C. Qu, J. M. Bowman, R. W. Field and A. G. Suits, *J. Phys. Chem. Lett.*, 2015, **6**, 2457-2462.

36 R. Fernando, N. M. Ariyasingha and A. G. Suits, *Chem. Phys. Lett.*, 2016, **645**, 76-83.

37 L. R. McCunn, D. I. G. Bennett, L. J. Butler, H. Fan, F. Aguirre and S. T. Pratt, *J. Phys. Chem. A*, 2006, **110**, 843-850.

38 M. Kawasaki, K. Kasatani, H. Sato, H. Shinohara and N. Nishi, *Chem. Phys.*, 1984, **88**, 135-142.

39 Y.-R. Lee and S.-M. Lin, *J. Chem. Phys.*, 1998, **108**, 134-141.

40 C. D. Foley, B. S. Joalland, S. T. Alavi and A. G. Suits, *Phys. Chem. Chem. Phys.*, 2018, DOI: 10.1039/C8CP04596H.

41 D. Townsend, M. P. Minitti and A. G. Suits, *Rev. Sci. Instrum.*, 2003, **74**, 2530-2539.

42 D. S. Green, G. A. Bickel and S. C. Wallace, *J. Mol. Spectrosc.*, 1991, **150**, 303-353.

43 J. O. F. Thompson, C. Amarasinghe, C. D. Foley, N. Rombes, Z. Gao, S. N. Vogels, S. Y. T. van de Meerakker and A. G. Suits, *J. Chem. Phys.*, 2017, **147**, 074201.

44 J. O. F. Thompson, C. Amarasinghe, C. D. Foley and A. G. Suits, *J. Chem. Phys.*, 2017, **147**, 013913.

45 C. Abeysekera, L. N. Zack, G. B. Park, B. Joalland, J. M. Oldham, K. Prozument, N. M. Ariyasingha, I. R. Sims, R. W. Field and A. G. Suits, *J. Chem. Phys.*, 2014, **141**, 214203.

46 J. M. Oldham, C. Abeysekera, B. Joalland, L. N. Zack, K. Prozument, I. R. Sims, G. B. Park, R. W. Field and A. G. Suits, *J. Chem. Phys.*, 2014, **141**, 154202.

47 K. Prozument, G. B. Park, R. G. Shaver, A. K. Vasiliou, J. M. Oldham, D. E. David, J. S. Muenter, J. F. Stanton, A. G. Suits and G. B. Ellison, *Phys. Chem. Chem. Phys.*, 2014, **16**, 15739-15751.

48 K. Prozument, G. B. Park, R. G. Shaver, A. K. Vasiliou, J. M. Oldham, D. E. David, J. S. Muenter, J. F. Stanton, A. G. Suits, G. B. Ellison and others, *Phys. Chem. Chem. Phys.*, 2014, **16**, 15739-15751.

49 J.-D. Chai and M. Head-Gordon, *Phys. Chem. Chem. Phys.*, 2008, **10**, 6615-6620.

50 T. H. Dunning Jr, *J. Chem. Phys.*, 1989, **90**, 1007-1023.

51 T. H. Dunning Jr, K. A. Peterson and A. K. Wilson, *J. Chem. Phys.*, 2001, **114**, 9244-9253.

52 D. E. Woon and T. H. Dunning Jr, *J. Chem. Phys.*, 1993, **98**, 1358-1371.

53 J. A. Montgomery Jr, M. J. Frisch, J. W. Ochterski and G. A. Petersson, *J. Chem. Phys.*, 1999, **110**, 2822-2827.

54 J. W. Ochterski, G. A. Petersson and J. A. Montgomery Jr, *J. Chem. Phys.*, 1996, **104**, 2598-2619.

55 G. Petersson and M. A. Al-Laham, *J. Chem. Phys.*, 1991, **94**, 6081-6090.

56 M. J. Frisch, G. W. Trucks, H. B. Schlegel, G. E. Scuseria, M. A. Robb, J. R. Cheeseman, G. Scalmani, V. Barone, G. A. Petersson, H. Nakatsuji, X. Li, M. Caricato, A. V. Marenich, J.

Bloino, B. G. Janesko, R. Gomperts, B. Mennucci, H. P. Hratchian, J. V. Ortiz, A. F. Izmaylov, J. L. Sonnenberg, Williams, F. Ding, F. Lipparini, F. Egidi, J. Goings, B. Peng, A. Petrone, T. Henderson, D. Ranasinghe, V. G. Zakrzewski, J. Gao, N. Rega, G. Zheng, W. Liang, M. Hada, M. Ehara, K. Toyota, R. Fukuda, J. Hasegawa, M. Ishida, T. Nakajima, Y. Honda, O. Kitao, H. Nakai, T. Vreven, K. Throssell, J. A. Montgomery Jr., J. E. Peralta, F. Ogliaro, M. J. Bearpark, J. J. Heyd, E. N. Brothers, K. N. Kudin, V. N. Staroverov, T. A. Keith, R. Kobayashi, J. Normand, K. Raghavachari, A. P. Rendell, J. C. Burant, S. S. Iyengar, J. Tomasi, M. Cossi, J. M. Millam, M. Klene, C. Adamo, R. Cammi, J. W. Ochterski, R. L. Martin, K. Morokuma, O. Farkas, J. B. Foresman and D. J. Fox, Gaussian 16 Rev. B.01, Wallingford, CT, 2016.

57 R. N. Zare and D. R. Herschbach, *Proceedings of the IEEE*, 1963, **51**, 173-182.

58 T. P. Rakitzis and R. N. Zare, *J. Chem. Phys.*, 1999, **110**, 3341-3350.

59 C. M. Western, *J. Quant. Spectrosc. Ra.*, 2017, **186**, 221-242.

60 C. Western, *University of Bristol*, 2010, **7**, 108.

61 A. Burcat and B. Ruscic, *Third millenium ideal gas and condensed phase thermochemical database for combustion with updates from active thermochemical tables*, Argonne National Laboratory Argonne, IL, 2005.

62 B. Ruscic, R. E. Pinzon, M. L. Morton, G. von Laszevski, S. J. Bittner, S. G. Nijsure, K. A. Amin, M. Minkoff and A. F. Wagner, *J. Phys. Chem. A*, 2004, **108**, 9979-9997.

63 B. Joalland, Y. Shi, A. Kamasah, A. G. Suits and A. M. Mebel, *Nat. Commun.*, 2014, **5**, 4064.

64 B. Joalland, R. Van Camp, Y. Shi, N. Patel and A. G. Suits, *J. Phys. Chem. A*, 2013, **117**, 7589-7594.

65 B. M. Broderick, N. Suas-David, N. Dias and A. G. Suits, *Phys. Chem. Chem. Phys.*, 2018, **20**, 5517-5529.

TOC Graphic

High power IR excitation coupled with state resolved imaging of propargyl chloride shows both IR multiphoton dissociation and vibrationally-mediated photodissociation.